An asymmetry detected in the disk of Kappa CMa with the AMBER/VLTI

Anthony Meilland, Florentin Millour, Philippe Stee, Armando Domiciano de Souza, Romain G. Petrov, Denis Mourard, Slobodan Jankov, Sylvie Robbe-Dubois, Alain Spang, Eric Arisitidi, et al.

▶ **To cite this version:**

Anthony Meilland, Florentin Millour, Philippe Stee, Armando Domiciano de Souza, Romain G. Petrov, et al.. An asymmetry detected in the disk of Kappa CMa with the AMBER/VLTI. Astronomy and Astrophysics - A&A, 2007, 464 (1), pp.73. 10.1051/0004-6361:20065410 . hal-00114736

HAL Id: hal-00114736
https://hal.science/hal-00114736

Submitted on 17 Nov 2006

HAL is a multi-disciplinary open access archive for the deposit and dissemination of scientific research documents, whether they are published or not. The documents may come from teaching and research institutions in France or abroad, or from public or private research centers.

L'archive ouverte pluridisciplinaire **HAL**, est destinée au dépôt et à la diffusion de documents scientifiques de niveau recherche, publiés ou non, émanant des établissements d'enseignement et de recherche français ou étrangers, des laboratoires publics ou privés.

Astronomy & Astrophysics manuscript no. HD50013˙accepted.hyper15964 November 17, 2006
© ESO 2006

hal-00114736, version 1 - 17 Nov 2006

An asymmetry detected in the disk of κ CMa* with the VLTI/AMBER

A. Meilland[1], F. Millour[2,3], Ph. Stee[1], A. Domiciano de Souza[2,1], R.G. Petrov[2], D. Mourard[1], S. Jankov[2], S. Robbe-Dubois[2], A. Spang[1], E. Aristidi[2], P. Antonelli[1], U. Beckmann[4], Y. Bresson[1], A. Chelli[3], M. Dugué[1], G. Duvert[3], L. Glück[3], P. Kern[3], S. Lagarde[1], E. Le Coarer[3], F. Lisi[5], F. Malbet[3], K. Perraut[3], P. Puget[3], G. Weigelt[4], G. Zins[3], M. Accardo[5], B. Acke[3,12], K. Agabi[2], B. Arezki[3], E. Altariba[2], C. Baffa[5], J. Behrend[4], T. Blöcker[4], S. Bonhomme[1], S. Busoni[5], F. Cassaing[6], J.-M. Clausse[1], C. Connot[4], A. Delboulbé[3], T. Driebe[4], P. Feautrier[3], D. Ferruzzi[5], T. Forveille[3], E. Fossat[2], R. Foy[7], D. Fraix-Burnet[3], A. Gallardo[3], S. Gennari[5], A. Glentzlin[1], E. Giani[5], C. Gil[3,13], M. Heiden[4], M. Heininger[4], O. Hernandez[3], K.-H. Hofmann[4], D. Kamm[1], S. Kraus[4], D. Le Contel[1], J.-M. Le Contel[1], B. Lopez[1], Y. Magnard[3], A. Marconi[5], G. Mars[1], G. Martinot-Lagarde[8,14], P. Mathias[1], J.-L. Monin[3], D. Mouillet[3,15], P. Mège[3], E. Nussbaum[4], K. Ohnaka[4], F. Pacini[5], C. Perrier[3], Y. Rabbia[1], S. Rebattu[1], F. Reynaud[9], A. Richichi[10], A. Roussel[1], M. Sacchettini[3], P. Salinari[5], D. Schertl[4], W. Solscheid[4], P. Stefanini[5], M. Tallon[7], I. Tallon-Bosc[7], D. Tasso[1], E. Tatulli[3], L. Testi[5], J.-C. Valtier[1], M. Vannier[2,11], N. Ventura[3], M. Kiekebusch[11], and M. Schöller[11]

(Affiliations can be found after the references)

Received; accepted

ABSTRACT

Aims. We study the geometry and kinematics of the circumstellar environment of the Be star κ CMa in the Brγ emission line and its nearby continuum.

Methods. We use the VLTI/AMBER instrument operating in the K band which provides a spatial resolution of about 6 mas with a spectral resolution of 1500 to study the kinematics within the disk and to infer its rotation law. In order to obtain more kinematical constraints we also use an high spectral resolution Paβ line profile obtain in December 2005 at the Observatorio do Pico do Dios, Brazil and we compile V/R line profile variations and spectral energy distribution data points from the literature.

Results. Using differential visibilities and differential phases across the Brγ line we detect an asymmetry in the disk. Moreover, we found that κ CMa seems difficult to fit within the classical scenario for Be stars, illustrated recently by α Arae observations, i.e. a fast rotating B star close to its breakup velocity surrounded by a Keplerian circumstellar disk with an enhanced polar wind. Finally we discuss the possibility for κ CMa to be a critical rotator with a Keplerian rotating disk and try to see if the detected asymmetry can be interpreted within the "one-armed" viscous disk framework.

Key words. Techniques: high angular resolution – Techniques: interferometric – Stars: emission-line, Be – Stars: Keplerian rotation – Stars: individual (κ CMa) – Stars: circumstellar matter

1. Introduction

The "Be phenomenon" is related to hot stars that have at least exhibited once Balmer lines in emission with infrared excess produced by free-free and free-bound processes in an extended circumstellar disk. There is now a strong evidence that the disk around the Be star α Arae is Keplerian (Meilland et al. 2006a) and that this dense equatorial disk is slowly expanding. On the other side there are also clear pieces of evidence for a polar enhanced wind. This was already predicted for almost critically rotating stars as for a large fraction of Be stars. Recently, Kervella & Domiciano de Souza (2006) showed an enhanced polar wind for the Be star Achernar whereas this Be star presents no hydrogen lines in strong emission. Thus, it seems that a significant polar wind may be present even if the star is still in a normal B phase, signifying this enhanced polar wind would not be related to the existence of a dense equatorial envelope. However many issues remain unsolved on the actual structure of the circumstellar envelopes in Be stars which probably depends on the dominant mass ejection mechanisms from the central star and on the way the ejected mass is redistributed in the near circumstellar environment. Recently Meilland et al. (2006b) reported theoretical spectral energy distributions (SEDs), Brγ line profiles and visibilities for two likely scenarii of the disk dissipation of active hot stars, and account for the transition from the Be to the B spectroscopic phase.

κ CMa (HD 50013, HR 2538) is one the brightest Be star of the southern hemisphere (V=3.8, K=3.6). It is classified as a B2IVe star, and the distance deduced from Hipparcos parallax is 230 ±30 pc. The measured vsini values range from 220 kms^{-1} (Dachs et al. 1989; Mennickent et al. 2004; Okazaki 1997; Prinja 1989) to 243 kms^{-1} (Zorec et al.2005) , its radius is 6 $R_\odot$ (Dachs et al. 1989; Prinja 1989) and its mass is 10 $M_\odot$ (Prinja 1989).

We must mention that the mass and radius determination of a Be star is not an easy task. For instance if we assume values of masses and radii from Harmanec (1988) compilation, in agreement with Schaller et al. (1992) non-rotating evolutionary models, for the effective temperatures used by Popper (1980), Prinja (1989) and Fremat (2005) we obtain the table 1.

T_{eff} in K	Mass in $M_\odot$	Normal Radius in $R_\odot$	Radius from parallax in $R_\odot$
20000	6.60	3.71	7.25 (6.46 - 8.24)
23100	8.62	4.28	6.26 (5.59 - 7.13)
25800	10.72	4.83	5.59 (4.98 - 6.36)

Table 1. Masses and radii determination for κ CMa from Harmanec (1988) compilation for the effective temperatures given by Popper (1980), Prinja (1989) and Fremat (2005).

Thus, for a main sequence star the stellar radius should be smaller than the 6 $R_\odot$ we have adopted but on the other side, our radius estimate based on the parallax and the chosen V magnitude from the correlation between the brightness and emission strength, as proposed by Harmanec (2000), gives the range of radii comparable to our chosen 6 $R_\odot$ used in our modeling.

The star exhibits a huge IR-excess and a strong emission in the hydrogen lines making a good candidate for the VLTI/AMBER spectro-interferometer (Petrov et al. (2006)) using medium spectral resolution (1500). Our aim is to study the geometry and kinematics of the circumstellar environment of this star as a function of wavelength, especially across the Brγ emission line and to detect any signature of a possible asymmetry of its circumstellar disk as already observed through a violet to red peaks ratio V/R ~ 1.3 by Dachs et al. (1992) and Slettebak et al. (1992).

Send offprint requests to: anthony.meilland@obs-azur.fr

⋆ Based on Guaranteed Time Observations made with the Very Large Telescope Interferometer at Paranal Observatory

2. Observations and data reduction

Dedicated observations of κ CMa were carried out during the night of the December, 26th 2004 with the three VLTI 8m ESO telescopes UT2, UT3 and UT4 (See Table 3 for the baseline configurations). The data were reduced using the amdlib (v1.15)/ammyorick (v0.54) software package developed by the AMBER consortium. It uses a new data processing algorithm adapted to multiaxial recombination instruments called P2VM for *Pixel To Visibility Matrix* algorithm. The squared visibility estimator is computed from the basic observable coming from this algorithm that is the coherent flux (i.e. complex visibilities frame by frame multiplied by the flux) and the estimated fluxes from each telescope. The principles of the general AMBER data reduction are described in more details by Millour et al. (2004) and Tatulli et al. (2006).

The complex coherent flux allows also to compute differential phase, i.e. averaged instantaneous phase substracted from achromatic atmospheric OPD and a wavelength-averaged reference phase. This means that the differential phase is the difference between the phase of the source complex visibility and a mean OPD. This leads to an average differential phase equal to zero on the observed spectral window and the lost of the object's phase slope over the wavelengths. This technique allows however to retrieve partial information of the object's phase and is almost equal to the object's interferometric phase if we have some spectral channels where we know the object's phase is zero.

Moreover, it also allows to compute "differential" visibility (as defined in Millour et al. 2006 and in Meilland et al. 2006a), i.e. the instantaneous modulus of the complex visibility divided by the averaged visibility on all the wavelengths excepted the work one. This leads to an average differential visibility equal to 1 in the continuum. It has the advantage over the "classical" visibility estimator to be almost insensitive to rapid frame to frame variations of visibility (due to vibrations or atmospheric jittering for example) and therefore one can expect the differential visibility observable to be more precise than the classical visibility estimator given the current vibrations in the VLTI infrastructure, and even though the continuum visibility information is lost in this observable.

For more information, the differential data reduction is described in details in Millour et al. (2005) and Millour et al. (2006).

Reducing the κ CMa data with a good accuracy was quite difficult to achieve. We encountered specific problems related to this data set. Therefore, in addition to the tools furnished by the default package, some specific processing was added to reach the best precision on the interferometric observables.

Table 2. Calibration stars diameters estimated from spectro-photometric indices (computed as in Bonneau et al. 2006) and their associated errors.

Star	Diameter (mas)	Error (mas)
HD 75063	0.50	0.08
HD 93030	0.454	0.006

– First of all, no specific data were available to calibrate the fringe contrast of κ CMa. We therefore looked at calibration stars observed during the same night for other stars and corrected their visibilities averaged over all the [2.13-2.21] μm observed spectral range from their estimated diameters (see table 2) in order to monitor the instrumental+atmospheric transfert function (see Fig. 1). This transfert function is the visibility of a point source measured by the instrument, allowing us to correct the raw visibilities on the science star from the instrumental-specific visibility loss. The scattering over the time of the visibilities gives the dispersion due to the instrumental drifts and atmospheric fluctuations during the observing time. This leads to a visibilities dispersion estimate of 0.05 for each star, which leads to an error on calibrated visibilities of 0.07 ($\sqrt{2 \times 0.05^2}$).
Then we interpolate the estimated transfert function to the time of the science star observations (as in Perrin et al. 2003). By using this technique, we find that the [2.13-2.21] μm averaged visibility of κ CMa is really close to 1.0 with

an uncertainty of 0.07 on all the observed base lengths. This would normally be killing for the wavelength-dependence study of the visibilities, but as explained before, we expect to have differential visibility and differential phase estimators much more precise than the visibility estimator.

– The lack of dedicated calibration star for κ CMa should have lead to an unfeasibility to spectrally calibrate the differential observables, but fortunately an other calibration star (HD93030) was observed two hours later within almost the same spectral window, which means that the spectrograph grating did not move but that the detector window was not exactly the same as for κ CMa, allowing us to use the intersecting spectral channels between the two observations without any calibration problem. Detailed data analysis of calibration stars tends to demonstrate that the main pattern on differential observables comes from a fiber-injection pattern (i.e. a pure internal AMBER instrumental effect) and that it is stable over several minutes in the 10^{-2} range for the differential visibilities and 10^{-2} radians for the differential phase at medium spectral resolution (R $\sim$ 1500, see for instance Vannier et al., 2005).

This allowed us to calibrate correctly the differential visibility and the differential phases (See Fig. 2). In order to ensure our calibration, we checked that all the features mentioned in this article are already present in the uncalibrated data, and not added by pure noise-effects produced by the calibrator star.

We could expect to see an effect in the closure phase, but its modulation seems to be of the order of amplitude of the error bars (3 °or 0.05 radians), which means that we do not see any detectable signal in the closure phase. This non-detection confirms the result on the visibility and the low amplitude of the modulation on the differential phases: the object is almost non-resolved or barely resolved by the interferometer on the considered baselines (80m maximum).

What we see in the observed data is a decrease in the differential visibilities in two of the three baselines of the order of 0.07, much larger than the error bars (0.02 for the differential visibilities). This can be explained by an envelope larger than the star, visible in the emission line.

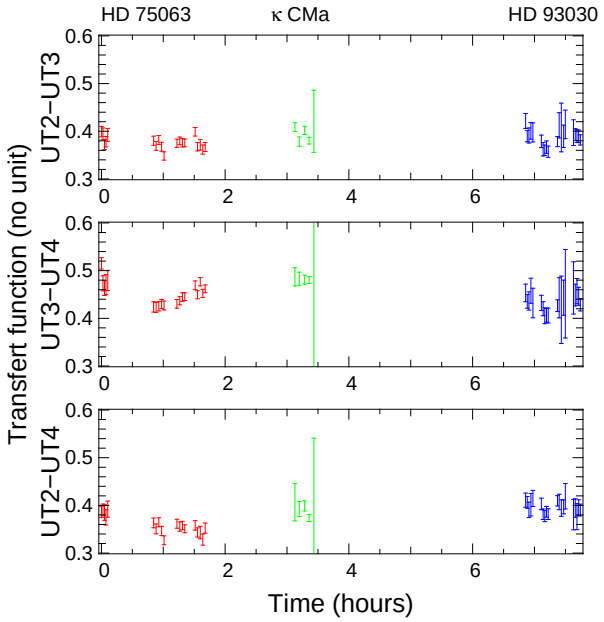

Fig. 1. Raw absolute visibilities of calibration stars corrected from their angular diameters and averaged over the [2.13-2.21] μm window, allowing us to monitor the instrumental+atmospheric transfert function (points respectively around 1h in red and 7h in blue). We have overplotted for comparison the raw visibilities of κ CMa (around 3h in green). The κ CMa visibilities have obviously the same value as the instrumental+atmospheric transfert function within the error bars, leading to a calibrated visibility of 1, i.e. a non resolved or very barely resolved object on all baselines.

We observe also a modulation in the differential phase of the order of 5°(0.09 radians), also higher than the error bars (2°or 0.03 radians). The modulation of the differential phase show a “sine arch” shape, typical of a rotating object or a bipolar outflow but also show an asymmetry, mainly on the baseline UT2-UT3 (B1).

In order to obtain more kinematical constraints the star has also been observed in the J2 band (1.2283-1.2937μm) with the 1.6 m Perkin-Elmer telescope and Coudé spectrograph (with R=10 000) at the Observatório do Pico dos Dias, Laboratório Nacional de Astrofísica (LNA), Itajubá, Brasil. The spectra

were recorded in the night 20/21 November 2005, at seven different positions along the slit using the Câmara Infravermelho (CamIV) detector. The images of the dark have been subtracted from each star's spectral image, wavelength calibration image and five flat-field images. To get the sky image we made the median combination of the star's spectral images (divided previously by the average of flat-field images). The sky image has been subtracted from stellar images and the one-dimensional spectra were extracted and calibrated in wavelength using the standard IRAF [1] procedures. Finally the continuum normalization around the Paβ line has been performed using our software. The average profile of the line, which has been used to constrain the kinematics within the disc, is plotted in Fig. 2 and 5.

3. Envelope extension and flattening

In this section we present the AMBER data in order to obtain an estimate of the κ CMa's envelope geometry and extension. Assuming that the measured visibility in the continuum, V_c, is only due to the central star and its circumstellar envelope and that the envelope is optically thin in the continuum, we can write:

$$V_c = \frac{V_{ec}F_{ec} + V_\star F_\star}{F_c} \quad (1)$$

where V_{ec} and F_{ec} are respectively the envelope visibility and flux in the continuum, $V_\star$ and $F_\star$ are the star visibility and flux in the continuum and $F_c = F_{ec}+F_\star$.

The total flux is normalized, i.e. $F_c = F_{ec} + F_\star = 1$. Since the star is fully unresolved $\phi_\star \sim 0.25$mas (assuming a 6 $R_\odot$ seen at 230 pc) which corresponds to $V_\star > 0.99$ for the longest baseline at 2.1 μm, we assume in the following that $V_\star$=1. In order to estimate V_{ec} we still have to determine the star and the envelope contributions at 2.1 μm. Using the fit of the SED given in Fig. 3 we estimate that at this wavelength the stellar emission is similar to the envelope contribution, i.e. $F_\star = F_{ec} = 0.5$.

We have the same relation for the visibility in the Brγ line:

$$V_r = \frac{V_{er}F_{er} + V_cF_c}{F_r} \quad (2)$$

where V_r and F_r are respectively the measured visibility and flux in the Brγ line. V_c and F_c are previously defined and V_{er} and F_{er} are the visibility and flux only due to the Brγ line, i.e. without any stellar contribution and envelope continuum. Using the AMBER Brγ emission line profile plotted in Fig. 2 and neglecting the underlying broadened photospheric absorption line, we obtain F_{er}=0.5 and F_r=1.5 at the center of the line.

The corresponding visibilities, deduced from Eq. 1 and 2 and from the measurements shown in Fig. 2, are given in Table 3. Using a uniform disk model for the envelope contribution, for each measurement, we also estimate in Table 3 the corresponding angular diameters in the continuum and in the Brγ line. Since the envelope is marginally resolved in the continuum we simply put an upper limit to its angular size.

The envelope extensions in Brγ given in Table 3 are strongly dependent on the sky-plane baseline orientation as seen in Fig. 4, where we plotted the κ CMa (unresolved star + uniform disk) model diameters as a function of the baseline orientation.

The κ CMa circumstellar disk seems to be elongated along B_1 but since we only have 3 visibility measurements we cannot accurately determine the angular position of the major-axis assuming an elliptical circumstellar disk. The envelope flattening given by the semi-major and semi-minor axis ratio, is about 2±0.7. Assuming that the disk is geometrically thin (i.e. its opening angle is only a few degree) we can estimate the range for the inclination angle i: 39°<i<68°. The lower limit of 39° relies on the lack of constraint on the disk opening angle.

4. SIMECA modeling

In order to obtain quantitative fundamental parameters of the central star and its circumstellar disk, we used the SIMECA code developed by Stee (1994) and Stee & Bittar (2001) to

[1] IRAF is distributed by the National Optical Astronomy Observatories, which is operated by the Association of Universities for Research in Astronomy (AURA), Inc., under cooperative agreement with the National Science Foundation.

Base n^o	1	2	3
Baseline	UT2-3	UT3-4	UT2-4
Length (m)	42.7	59.3	80.8
P.A. (°)	51.6	128	97.1
V_c	>0.93	>0.93	>0.93
V_r/V_c	0.93±0.02	0.95±0.02	0.9±0.02
V_r	0.85<V_r<0.95	0.87<V_r<0.97	0.82<V_r<0.92
V_{ec}	>0.86	>0.86	>0.86
V_{er}	0.69<V_{er}<0.85	0.75<V_{er}<0.91	0.60<V_{er}<0.76
ϕ_{ec} (mas)	<3.6	<2.6	<1.9
ϕ_{er} (mas)	3.7<ϕ_{er}<5.5	2.0<ϕ_{er}<3.6	2.6<ϕ_{er}<3.4
ϕ_{ec} ($D_\star$)	<15.5	<11.2	<8.2
ϕ_{er} ($D_\star$)	15.9<ϕ_{er}<23.7	8.6<ϕ_{er}<15.4	11.2 <ϕ_{er}<14.6

Table 3. Brγ Visibilities measured in the continuum (V_c) and visibility drop within the Brγ line (V_r/V_c). V_r calculated from the measured V_c and V_r/V_c ratio. Deduced envelope contribution in the continuum (V_{ec}) and in the line (V_{er}) for each baseline. The corresponding angular diameters in the Brγ line (ϕ_{er}) and the nearby continuum (ϕ_{ec}) are computed using a uniform disk model for each envelope measurement. The corresponding extension in stellar radii are also given, assuming a $6R_\odot$ star at 230pc.

model the κ CMa circumstellar environment. Since this code was axi-symmetric we made substantial modifications in order to introduce a longitudinal dependence of the envelope density as evidenced from the AMBER data plotted Fig. 2. To constrain the kinematics within the disk we use a Paβ line profile obtained in December 2005 at the Observatorio do Pico do Dios, Brazil and plotted in Fig. 5. This profile is strongly asymmetric with a V/R double peak ~1.3. This V/R > 1 is usually interpreted in terms of a viscous disk similar to accretion disks where the gas and angular momentum are diffused outward by magnetohydrodynamic viscosity (Lee et al. 1991). Considering the time-dependent structure of isothermal viscous disk, Okazaki (1997) showed that "one-armed" density waves can propagate within the disk and should reproduce the observed V/R variations from V/R>1 to V/R<1 seen in the line profiles (Hummel & Hanuschik 1997). Such variations were detected for many Be stars, with period from a few years to over a decade (Hanuschik et al.1995; Telting et al. 1994). But in the case of κ CMa the V/R ratio has remained constant for the last twenty years (Dachs et al. 1992; Slettebak 1992).

In figure 5 we over-plotted the supposed "symmetric part" of the Paβ line profile, using an axi-symmetric model, and the asymmetric residual that may be produced within the "one-armed" oscillation over-density. This effect must be compatible with the asymmetric differential phase variation across the Brγ line for the B_1 baseline plotted in the bottom part of Fig. 5 since the emitting regions in Paβ and Brγ must be very close each together. The asymmetric contribution to the Brγ emission is about 20 to 30% of the total emission in this line whereas the mean projected velocity of the inhomogeneity is -130±20 kms^{-1}. Using a SIMECA model at 230pc we determined that the projected separation between this over-density photocenter and the central star is about $6.5_\star$.

The parameters obtained for our best model are given in Table 4 with the corresponding spectroscopic and interferometric observables of Fig. 2. This best model includes an over-density along the disk major axis at +20°, corresponding to an over-luminosity of 30% of the total flux in the line, and the agreement with the VLTI/AMBER data, the SED (Fig. 3) and the Paβ line profile is very good as it can be seen Fig. 2. The very nice agreement with the differential visibility and phase across the Brγ line for the three bases validates the chosen disk geometry and kinematics. The 2.1μm continuum visibilities obtained with the 3 baselines, respectively V_1=0.92, V_2=0.96 and V_3=0.94 are also compatible with the 0.93 lower limit measured with AMBER. The corresponding continuum intensity map in the continuum at 2.15 μm is plotted Fig. 6. The evaluation on the uncertainties of the parameters of our model is far below the scope of this letter and will be studied in depht as soon as we get more constraining data.

5. Discussion

Following recent VLTI/AMBER and VLTI/MIDI observations of α Arae Meilland et al. (2006a) concluded that this classical Be star fits very well within the classical scenario for the "Be phenomenon", i.e. a fast rotating B star close to its breakup

parameter	value
$T_{\rm eff}$	22 500 K ± 1000
Radius	6 $R_\odot$ ± 1
Inclination angle i	60° ± 10
Equatorial rotation velocity	240 km s^{-1} ± 20
rotation law exponent	0.32 ± 0.1
Photospheric density (ρ_{phot})	4. 10^{-11}g cm^{-3} ± 2 10^{-11}
Equatorial terminal velocity	1 km s^{-1} ± 10
Polar terminal velocity	1000 km s^{-1} ± 100
Polar mass flux	2 $10^{-11}M_\odot$ $year^{-1}$ sr^{-1} ± 0.5 10^{-11}
m1	10 ± 5
m2	10 ± 2
C1	30 ± 10
Envelope outer radius	23 $R_\star$ ± 2
Major axis position	+28° ± 5
Over-density position	along the disk major axis

Table 4. Parameters for the κ CMa central star and its circumstellar environment for the best axi-symetric model

velocity surrounded by a Keplerian circumstellar disk with an enhanced polar wind. This scenario was also confirmed for the Be star Achernar by Kervella & Domiciano de Souza (2006) using VLTI/VINCI data, even if, for this latter case, the star was not in its active Be phase, i.e without any strong emission line and no circumstellar disk. Nevertheless, Achernar was still a nearly critical rotator and was still exhibiting an enhanced polar stellar wind. We will see in the following that κ CMa does not fit very well within this classical scenario.

5.1. Is κ CMa a critical rotator ?

If κ CMa was rotating close to its breakup velocity, i.e. V_c=463kms^{-1}, the inclination angle would be around 28° in order to obtain a measured vsini =220 kms^{-1}). With this inclination angle the maximum flattening corresponding to a geometrically very thin disk is 1.12. Since we measure a flattening of about 2±0.7 this inclination angle can be ruled out. In our best SIMECA model the star is rotating at only 52% of its critical velocity. We may argue that the measured elongation is not the envelope major axis but rather the enhanced polar wind. In this case the projected axis of the Be envelope is not identical to the rotation axis of the star. Nevertheless, in order to obtain an asymmetry in the jet we need an extended optically thick disk, perpendicular to the jets directions, that may screen a least one part of the jet-like structure. Such extended optically thick disk should have been detected with the AMBER instrument which is not the case in our data.

The value of the projected rotational velocity for an early-B star can be systematically affected by pseudo-photosphere, unrecognized optically thick parts of the Be envelope as shown by Harmanec (2002) for γ Cas. He obtains for this star a vsini of 380 kms^{-1} instead of the often quoted value of 230 kms^{-1} from Sletteback (1992). Nevertheless, taking the largest value for κ CMa from the literature from Zorec (2005) who found a vsini=243kms^{-1} we still obtain an inclination angle of 32° which again is not in agreement with our measured flattening. Of course, if the discrepancy between the measured vsini and the "real" one is larger it may be possible that κ CMa is still a critical rotator but it requires a factor of 2 between the measured and the true vsini which we found unrealistic. Even if Townsend et al. (2004) include the gravity darkening effect on the vsini values of rigid early-type rotators, assuming a rotation rate Ω/Ω_c of 0.95, they conclude that classic vsini determinations for B0 to B9-type stars can be underestimated by 12 to 33%, far from a factor of 2. Moreover, a recent paper by Frémat et al.(2005) studying the effect of the gravitational darkening on the determination of fundamental parameters in fast rotating B-type stars found that on average the rate of angular velocity of Be stars attains only Ω/Ω_c~0.88.

In this last paper, Frémat et al.(2005) estimate κ CMa's effective temperature to be 25790 ± 713 K, a value significantly larger than the 22500 K used in our modeling. Moreover, Harmanec (2000) found a positive correlation between the emission strength and brightness in the optical. Therefore we may use the minimum observed V magnitude of about 3.5 to estimate the radius of the central star. Combining with the

Hipparcos parallax and its error we obtain a radius between 9 and 14 solar radii. Using the T_{eff} of 25790 K and a radius of 14 $R_\odot$ we obtain a stellar luminosity larger by a factor 8 compared to our modeling and thus it is not possible to obtain a good agreement with the observed SED plotted Fig.3. Thus we are more confident with our 6 $R_\odot$ used for our modeling and our finding that κ CMa seems not to be a critical rotator. Nevertheless, regarding the uncertainties and the large errors of all measurements the breakup velocity cannot be totally excluded.

5.2. Is the rotation law within the disk Keplerian ?

A Keplerian rotating law would produce a narrower double-peak separation in the Paβ line profile. Using a simple axi-symmetric Keplerian disk model the double-peak separation would be about 90kms^{-1} whereas we measure an asymmetric double-peak separation of about 160kms^{-1}. Even if we subtract the emission of the over-density producing a larger double-peak separation by contributing to the V peak of the emitting Paβ line, we still obtain a double-peak separation of about 120kms^{-1} (see Fig. 5). The exponent of the rotation law used for our best SIMECA model is 0.32 whereas it should be 0.5 for a purely Keplerian disk.

We may argue that Be stars vary strongly in time and thus line profiles shapes are time dependent. For instance actual Hα line profiles show a strong emission with a single peak whereas Bahng & Hendry (1975) saw a double-peaked Hα emission line, with the same double-peak separation of 160 km^{-1} we obtained for Paβ, with a shell core on their high-dispersion spectra. Nevertheless, these line variations are certainly related to the formation and disappearance of the circumstellar disk around the star as shown by Rivinius et al. (2001) and Meilland et al. (2006b). Whatever the model is, a double-peak line profile is a clear signature of an extended rotating disk, at least if the kinematics is not dominated by a strong stellar wind in the equatorial region as shown by Stee & de Araùjo (1994). This double-peak separation is a good indication of the disk extension as shown by Huang (1972); Hirata & Kogure (1984) and Stee & de Araùjo (1994). We measure v_{disk} sini at the disk outer radius (R_{disk}) from the peaks separation, where v_{env} is the rotational disk velocity at R_{disk}. Thus we can write:

$$v_{disk}\sin(i) = v_\star \sin(i)\left(\frac{R_{disk}}{R_\star}\right)^{-\beta}, \quad (3)$$

where $v_\star$ is the star rotation at its photosphere.

Assuming a Keplerian rotation (β =0.5) we obtain, using Eq. 3, R_{disk}=13.5 $R_\star$ which is about 2σ from the 19.8 $R_\star$ interferometric measurement, assuming that the measured elongation is the envelope major axis and not an enhanced polar wind (see discussion in the previous point). Note that these 19.8 $R_\star$ found are obtained assuming a uniform disk for the envelope and thus is certainly a lower limit to the "true" disk extension in the Paβ line. Thus it seems difficult to maintain a Keplerian rotation within the disk of κ CMa.

5.3. Is the "one-armed" viscous disk model a possible scenario for κ CMa ?

The asymmetry presently detected in the disk of κ CMa seems to be hardly explained within the "one-armed" viscous disk framework. Following the viscous disk models by Okazaki (1997) and the observational detection of "one-armed" oscillations in the disk of ζ Tau by Vakili et al. (1998) and γ Cas by Berio et al. (1999), the precessing period (P) of such oscillations should be confined within a few years up to about twenty years for the longer ones. On the other side, we tried to compile all the observational data available in order to obtain a "quasi-period" for the V/R variations. First we must mention that the V/R variations occur during the time intervals of observable presence of Be envelopes and that they can show long-term, medium-term as well as rapid changes (Dachs 1981). Moreover, the very strong Hα line profile is not really suitable to V/R measurements since it is single-peaked and the illusion of apparent V/R changes can be related to the presence of telluric lines. Finally, compiling the data between 1965 and 2003 for κ CMa respectively from Jaschek (1965), Slettebak (1982), Banerjee (2000) and this work, we were not

able to deduce an estimation of a quasi-period (Fig. 7). Several authors suggested a very long V/R variation (i.e. Okazaki P>28 years). This is a possibility but an equally plausible possibility is that the star had two episodes of V/R changes with much shorter cycle length separated by a period of quiescence documented by Dachs et al. 1992; Slettebak 1992. More observations are needed since, if this first possiblity could be confirmed, then there is a problem for the one-armed model. This "pseudo-period" would be too long compared to theoretical predictions which can be hardly longer than two decades for a disk with a radius $\sim 23 R_\star$ (Okazaki, private communication). Moreover, the fact that this over-density remains confined along the major axis of the disk seems to be a very nice coincidence...

Clearly, further observations are mandatory to confirm these conclusions or to see if other physical phenomena occurred within the circumstellar disk of κ CMa.

Acknowledgements. We thanks Atsuo Okasaki for his useful comments about the viscous discs models. We acknowledge the remarks of the referee Petr Harmanec which help to greatly improve the paper. We thank David Chapeau and Damien Mattei for the SIMECA code developments support.

The AMBER project has benefited from funding from the French Centre National de la Recherche Scientifique (CNRS) through the Institut National des Sciences de l'Univers (INSU) and its Programmes Nationaux (ASHRA, PNPS). The authors from the French laboratories would like to thank the successive directors of the INSU/CNRS directors. The authors from the the Arcetri Observatory acknowledge partial support from MIUR grants and from INAF grants. C. Gil work was supported in part by the Fundação para a Ciência e a Tecnologia through project POCTI/CTE-AST/55691/2004 from POCTI, with funds from the European program FEDER.

This research has also made use of the ASPRO observation preparation tool from the JMMC in France, the SIMBAD database at CDS, Strasbourg (France) and the Smithsonian/NASA Astrophysics Data System (ADS). This publication makes use of data products from the Two Micron All Sky Survey.

The AMBER data reduction software `amdlib` has been linked with the open source software Yorick[2] to provide the user friendly interface `ammyorick`. They are freely available on the AMBER website `http://amber.obs.ujf-grenoble.fr`.

[2] `http://yorick.sourceforge.net`

References

Bahng J.D.R. & Hendry E. 1975, PASP, 87, 137
Banerjee, D.P.K., Rawat, S.D. & Janardhan, P. 2000, A&AS, 147, 229
Berio, Ph., Stee, Ph., Vakili, F. et al. 1999, A&A 345, 203
Bonneau, D.; Clausse, J.; Delfosse, X. et al. 2006, A&A, 4469
Dachs, J., Eichendorf, W., Schleicher, H. et al. 1981, A&AS, 43, 427
Dachs, J., Poetzel, R. & Kaiser D. 1989, A&AS, 78, 487
Dachs, J., Hummel, W. and Hanuschik R.W. 1992 A&AS 95, 437
Domiciano de Souza, A., Kervella, P., Jankov, S. et al. 2003, A&A, 407, L47.
Frémat, Y., Zorec, J., Hubert, A-M et al. 2005, A&A, 440, 305
Hanuschik, R.W., Hummel, W., Dietle, O. et al. 1995, A&A, 300, 163
Harmanec, P. 1988, BAICz, 39, 329
Harmanec, P. 2000, Alicante IAU Col. 175, ASP 214, 13
Harmanec, P. 2002, ASPC, 279, 221
Hirata, R. & Kogure, T. 1984, Bull. Astr. Soc. India, 12, 109
Huang, S. 1972, ApJ, 171, 549
Hummel, W. & Hanuschik, R.W. 1997, A&A, 320, 852
Jaschek, C. and Jaschek M. 1965, PASP 77, 376
Kervella, P. & Domiciano de Souza, A. 2006, A&A, in press
Lee, U., Osaki, Y. & Saio, H. 1991, MNRAS, 250, 432
Marlborough, J.M. and Peters, G.J. 1986, ApJ Sup. Ser., 62, 875
Meilland, A., Stee, Ph., Vannier, M. et al. 2006a, A&A, in press
Meilland, A., Stee, Zorec, J. et al. 2006b, A&A, 455, 953
Mennickent, R.E., Vogt, N., Barrera, L.H. 1994, A&AS, 106, 427
Millour, F., Tatulli, E., Chelli, A. et al. SPIE 2004, 5491, 1222
Millour, F., Vannier, M., Petrov, R.G et al. 2005, EAS Publications Series, in press

Millour, F., Petrov, R. G, Chesneau, O. et al. 2006, A&A, accepted.
Okazaki, A., 1997, A&A 318, 548
Petrov, R. G, Malbet, F., Antonelli, P. et al. 2006, A&A, submitted.
Perrin, G. 2003, A&A, 400, 1173
Popper, D.M. 1980, ARA&A, 18, 115
Prinja R.K. 1989, MNRAS, 241, 721
Rivinius, Th., Baade, D., Stefl, S. et al. 2001, A&A, 379, 257
Schaller, G., Schaerer, D., Meynet, G. et al. 1992, A&AS, 96, 269
Slettebak, A. 1982, ApJ, 50, 55
Slettebak, A., Collin, G., et al., 1992, ApJS 81, 335
Stee, Ph., de Araùjo, F.X. 1994, A&A, 292, 221
Stee, Ph., de Araùjo, F.X., Vakili F. et al. 1995, A&A, 300, 219
Stee, Ph. and Bittar, J. 2001, A&A, 367, 532
Tatulli, E., Millour, F., Chelli, A. et al. 2006, A&A, in press
Telting, J.H., Heemskerk, M.H.M., Henrichs, H.F. et al. 1994, A&A, 288, 558
Townsend, R.H.D., Owocki, S.P., & Howarth, I.D. 2004, MNRAS, 350, 189
Vannier, M., Millour, F. and Petrov, R.G. in *The power of optical/IR interferometry*, ESO conf, 2005, in press.
Vakili, F., Mourard, D., Stee, Ph., et al. 1998, A&A 335, 261
Zorec, J., Frémat, Y. & Cidale, L. 2005, A&A, 441, 235

[1] Laboratoire Gemini, U.M.R. 6203 Observatoire de la Côte d'Azur/C.N.R.S., Avenue Copernic, 06130 Grasse, France
[2] Laboratoire Universitaire d'Astrophysique de Nice, UMR 6525 Université de Nice/CNRS, Parc Valrose, F-06108 Nice cedex 2, France
[3] Laboratoire d'Astrophysique de Grenoble, U.M.R. 5571 Université Joseph Fourier/C.N.R.S., BP 53, F-38041 Grenoble Cedex 9, France
[4]
[5] Max-Planck-Institut für Radioastronomie, Auf dem Hügel 69, D-53121 Bonn, Germany
[6] INAF-Osservatorio Astrofisico di Arcetri, Istituto Nazionale di Astrofisica, Largo E. Fermi 5, I-50125 Firenze, Italy
[7] ONERA/DOTA, 29 av de la Division Leclerc, BP 72, F-92322 Chatillon Cedex, France
[8] Centre de Recherche Astronomique de Lyon, UMR 5574 Université Claude Bernard/CNRS, 9 avenue Charles André, F-69561 Saint Genis Laval cedex, France
[9] Division Technique INSU/CNRS UPS 855, 1 place Aristide Briand, F-92195 Meudon cedex, France
[10] IRCOM, UMR 6615 Université de Limoges/CNRS, 123 avenue Albert Thomas, F-87060 Limoges cedex, France
[11] European Southern Observatory, Karl Schwarzschild Strasse 2, D-85748 Garching, Germany
[12] European Southern Observatory, Casilla 19001, Santiago 19, Chile
[13] Instituut voor Sterrenkunde, KULeuven, Celestijnenlaan 200B, B-3001 Leuven, Belgium
[14] Centro de Astrofísica da Universidade do Porto, Rua das Estrelas - 4150-762 Porto, Portugal
[15] *Present affiliation:* Observatoire de la Cte d'Azur - Calern, 2130 Route de l'Observatoire , F-06460 Caussols, France
[16] *Present affiliation:* Laboratoire Astrophysique de Toulouse, UMR 5572 Université Paul Sabatier/CNRS, BP 826, F-65008 Tarbes cedex, France

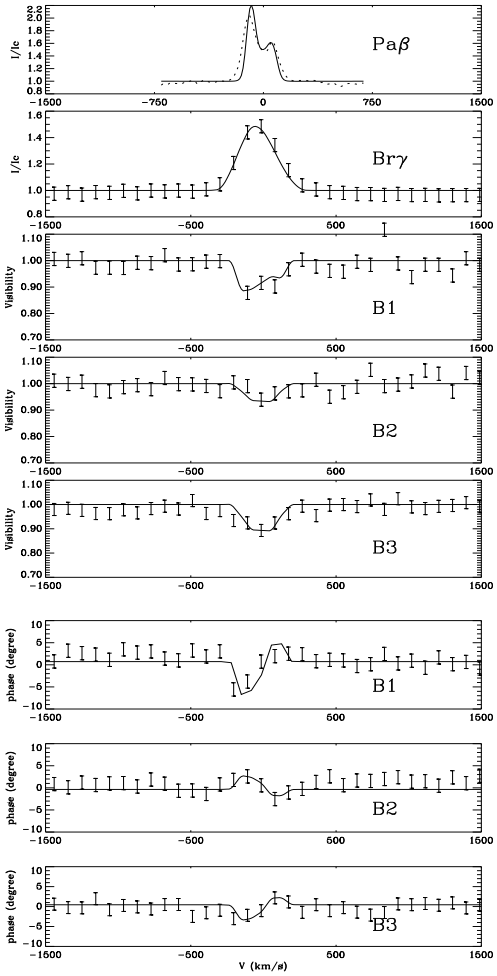

Fig. 2. From the top to bottom : Paβ line profile from the Observatorio do Pico dos Dias, Brazil (dotted line) with our best model fit (plain line), Brγ line profile, differential visibilities and differential phases for the three baselines. For each plot, the dots with errors bars are VLTI/AMBER data and the solid line is from our best SIMECA model (see section 4).

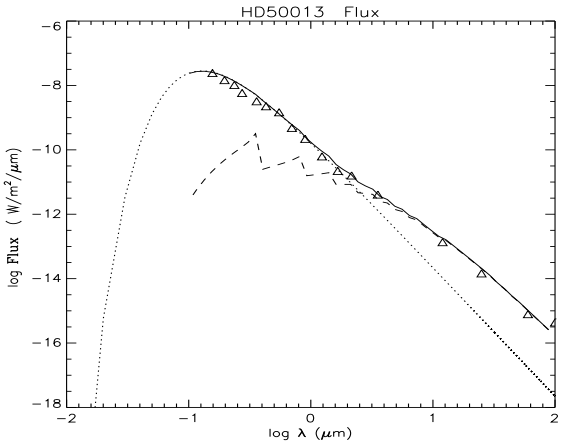

Fig. 3. κ CMa's Spectral Energy Distribution (SED) from SIMBAD CDS (triangles). Dotted line: emission from the central star assuming a black body with $R_\star = 6R_\odot$, T_{eff}=22500K and d=230 pc. Dashed line : free-free and free-bound envelope contribution from the SIMECA code between 0.3 and 100 μm . Plain line : Central star emission + envelope contribution.

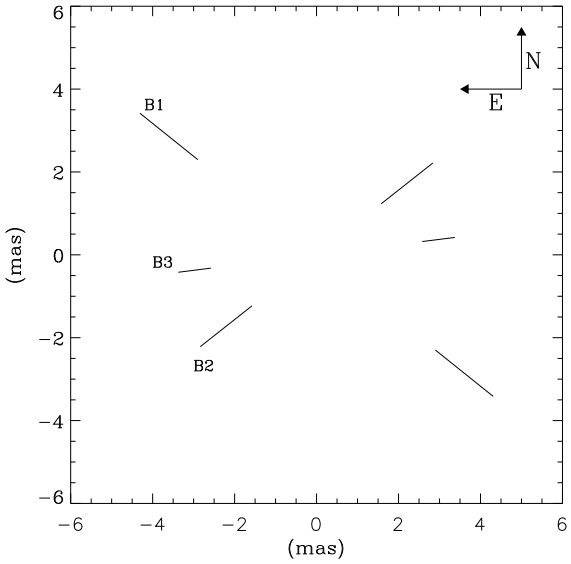

Fig. 4. κ CMa diameters in the Brγ line, assuming an unresolved star + uniform disk models, as a function of the baseline position angle (in mas). The length of each plot corresponds to the error bar measurement whereas diameters are given by the center of each error bar.

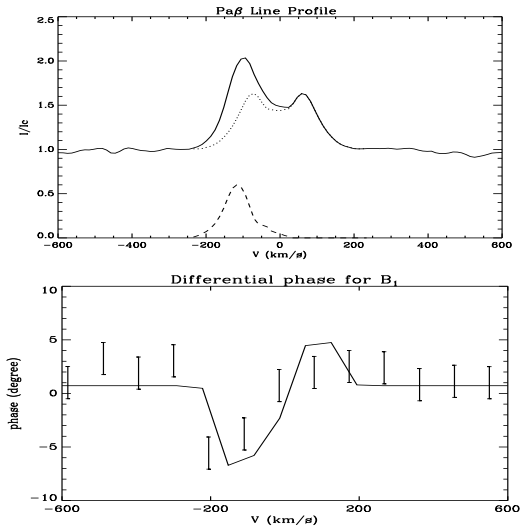

Fig. 5. Upper picture: κ CMa Paβ line profile observed in December 2005 at the Observatorio do Picos dos Dias, Brazil (solid line). Estimated symmetric part of the Paβ profile (dotted line) using an axi-symmetric model. The asymmetric residue corresponds to the emission of "one-armed" over-density (dashed line). Bottom picture: Differential phase variation measured along the B_1 baseline (dots with errors bars) and theoretical phase from the SIMECA code.

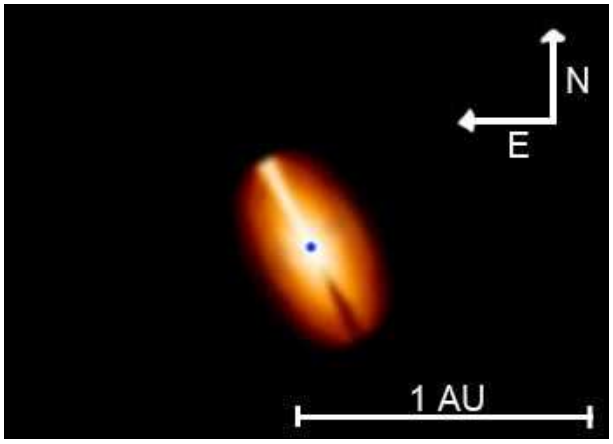

Fig. 6. Intensity map in the continuum at 2.15 μm obtained with SIMECA for our best model parameters. The inclination angle is 60°, the central black dot represents the κ CMa photosphere (0.25 mas), the bright part in the equatorial disk is produced by the over-density which is oriented along the B_1 baseline. This over-density is also responsible for a 30% emission excess in the asymmetric V part of the Brγ line.

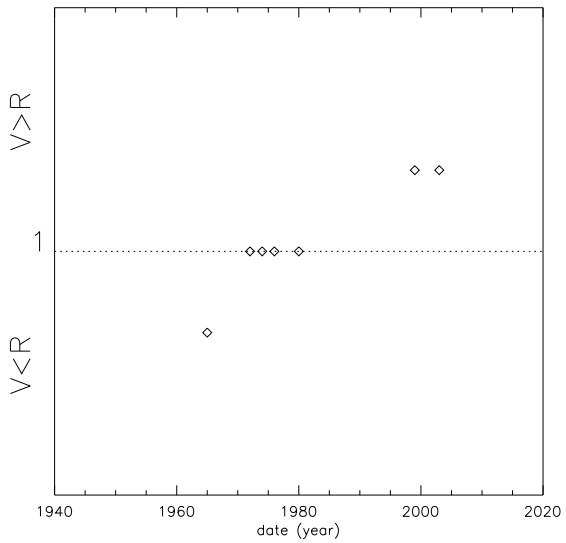

Fig. 7. V/R variations obtained from the literature between 1965 and 2003, respectively from Jaschek (1965), Slettebak (1982), Banerjee (2000) and this work.